

Article

## Fermi Surface Reconstruction due to Hidden Rotating Antiferromagnetism in N and P-Type High- $T_C$ Cuprates

Mohamed Azzouz

Department of Physics, Laurentian University, Ramsey Lake Road, Sudbury, Ontario P3E 2C6, Canada; E-Mail: mazzouz@laurentian.ca; Tel.: +1-705-675-1151 (ext. 2224); Fax: +1-705-675-4868

Received: 13 December 2012; in revised form: 17 April 2013 / Accepted: 18 April 2013 /

Published: 7 May 2013

---

**Abstract:** The Fermi surface calculated within the rotating antiferromagnetism theory undergoes a topological change when doping changes from p-type to n-type, in qualitative agreement with experimental data for n-type cuprate  $\text{Nd}_{2-x}\text{Ce}_x\text{CuO}_4$  and p-type  $\text{La}_{2-x}\text{Sr}_x\text{CuO}_4$ . Also, the reconstruction of the Fermi surface, observed experimentally close to optimal doping in p-type cuprates, and slightly higher than optimal doping in the overdoped regime for this n-type high- $T_C$  cuprate, is well accounted for in this theory. This reconstruction is a consequence of the quantum criticality caused by the disappearance of rotating antiferromagnetism. The present results are in qualitative agreement with recently observed quantum oscillations in some high- $T_C$  cuprates. This paper presents new results about the application of the rotating antiferromagnetism theory to the study of the electronic structure for n-type materials.

**Keywords:** rotating antiferromagnetism; high- $T_C$  cuprates; hidden order; symmetry breaking; fermi surface reconstruction

---

### 1. Introduction

The topology and doping dependence of the Fermi surface (FS) of high-temperature superconductors (HTSC) are currently highly debated. Some observations from angle-resolved-photoemission spectroscopy (ARPES) experiments do not seem to see any FS reconstruction, but data collected from magnetoresistance measurements characterized by Shubnikov-de Haas (SdH) oscillations indicate that the FS undergoes a topology change due to some sort of symmetry breaking. Since no long range order has been observed so far in underdoped high-temperature superconductors (HTSCs), we proposed earlier that the FS reconstruction is caused by the hidden rotating antiferromagnetic order.

In the present work, we support this proposal by new results for n-type cuprates and argue in favor of the FS of HTSCs undergoing topology reconstruction at specific doping levels in the framework of rotating antiferromagnetism theory (RAFT) [1]. We compare the evolution of the FS with doping in p-type and n-type HTSCs obtained in this theory and discuss it in connection mainly with available experimental data for n-type material  $\text{Nd}_{2-x}\text{Ce}_x\text{CuO}_4$  and p-type one  $\text{La}_{2-x}\text{Sr}_x\text{CuO}_4$ . It is found that the change in the topology of the FS as one goes from the p-type cuprate to n-type material is well accounted for in RAFT. In the low-doping limit (underdoped regime), RAFT yields a small almost square FS centered around  $(\pi, 0)$  points for n-type  $\text{Nd}_{2-x}\text{Ce}_x\text{CuO}_4$  in qualitative agreement with SdH oscillations, which indicate the existence of a FS in the form of small pockets [2]. A careful look at the data of Armitage *et al.* [3] in Figure 3 of their work reveals a trend qualitatively consistent with our findings for n-type material  $\text{Nd}_{2-x}\text{Ce}_x\text{CuO}_4$  regarding the evolution of spectral weight away from  $(\pi, 0)$  and the formation of a larger FS as doping increases. A FS in the form of stretched elliptic pockets nearby the  $(\pi/2, \pi/2)$  points is, however, likely for p-type  $\text{La}_{2-x}\text{Sr}_x\text{CuO}_4$ . Indeed, Figure 5 of the ARPES work by Yoshida *et al.* [4] shows nicely the evolution of the FS with doping from what we interpret as stretched small pockets in the underdoped regime to large contours in the overdoped regime. RAFT reproduces the FS evolution qualitatively well with doping for this p-type material. Note that p-type cuprates were examined using RAFT in [5]. However, this is the first work based on RAFT, which deals with the electronic structure in an n-type cuprate. In RAFT, for both p-type and n-type materials, the critical value of doping where FS reconstruction occurs is given by the value where rotating antiferromagnetism vanishes. In p-type materials, this value coincides practically with optimal doping, but in n-type case, it occurs in the overdoped regime beyond optimal doping for superconductivity (SC).

This paper is organized as follows. In Section 2, RAFT is extensively reviewed. In Section 3, the rotating antiferromagnetic and superconducting parameters are calculated as a function of doping and temperature. In Section 4, the doping dependence of the electronic structure is calculated and compared to experimental data. Energy spectra *versus* the wavevector are calculated for several doping levels, and the FS is calculated using the occupation probability for doping levels in n-type and p-type cases. Conclusions and a discussion of existing experimental data are given in Section 5.

## 2. Review of Rotating Antiferromagnetism Theory

### 2.1. Normal State

We first focus on the normal (non-superconducting) state where we review the derivation of rotating antiferromagnetism (RAF). In Section 2.4, we will review the interplay between SC and RAF. Consider here the  $t$ - $t'$  Hubbard model in two dimensions:

$$H = -t \sum_{\langle i,j \rangle \sigma} c_{i,\sigma}^\dagger c_{j,\sigma} - t' \sum_{\langle\langle i,j \rangle\rangle \sigma} c_{i,\sigma}^\dagger c_{j,\sigma} + \text{h.c.} - \mu \sum_{i,\sigma} n_{i,\sigma} + U \sum_i n_{i\uparrow} n_{i\downarrow} \quad (1)$$

where  $\langle i, j \rangle$  and  $\langle\langle i, j \rangle\rangle$  designate nearest and second-nearest neighboring sites, respectively, and  $t$  and  $t'$  are electron hopping energies to the nearest and second-nearest neighbors, respectively. Note that

hopping to further neighbors was also considered [5] for more accurate comparison with the experiment. The interacting term in Hamiltonian (1) has been decoupled using:

$$Q_i = \langle c_{i,\uparrow} c_{i,\downarrow}^\dagger \rangle = -\langle S_i^- \rangle \equiv |Q| e^{i\phi_i} \quad (2)$$

and mean-field theory [1,5–9] was recently combined with the Heisenberg equation [10] in order to calculate the phase of this order parameter. To use the Heisenberg equation, the interacting term,  $Un_{i\uparrow}n_{i\downarrow}$ , was rewritten in terms of the spin ladder operators in the following way. In second quantization, where:  $S_i^+ = c_{i,\uparrow}^\dagger c_{i,\downarrow}$ , the onsite Coulomb repulsion,  $Un_{i\uparrow}n_{i\downarrow}$ , was, on one hand, written as:  $Un_{i\uparrow}n_{i\downarrow} = Un_{i\uparrow} - US_i^+ S_i^-$  and on the other hand as:  $Un_{i\uparrow}n_{i\downarrow} = Un_{i\downarrow} - US_i^- S_i^+$ . Summing then dividing by 2 gave the symmetric expression:  $Un_{i\uparrow}n_{i\downarrow} = \frac{U}{2}(n_{i\uparrow} + n_{i\downarrow}) - \frac{U}{2}(S_i^+ S_i^- + S_i^- S_i^+)$  [10]. The terms,  $S_i^+ S_i^-$  and  $S_i^- S_i^+$ , which are responsible for onsite spin-flip excitations, contribute by lowering energy for the sites that are partially occupied by the same density of spin up and down electrons. We decoupled this term in the mean-field theory using  $\langle S_i^- \rangle \equiv \langle c_{i,\downarrow}^\dagger c_{i,\uparrow} \rangle$ , which leads to a collective behavior for the spin-flips, and recovered the results obtained earlier in RAFT [1,5–9]. In this state, a spin flip process at site  $i$  is simultaneously accompanied by another one at another site,  $j$ ; the occurrence of spin flips becomes synchronized below a transition temperature, which was identified with the pseudogap (PG) temperature. In Section 2.3 below, an interpretation of RAF from a classical point of view will be given.

The parameter,  $Q_i$ , in Equation (2) is thus used to carry on a mean-field decoupling of the  $t$ - $t'$  Hubbard model (1). Consideration of the ansatz, where  $\phi_i - \phi_j = \pi$ , with  $i$  and  $j$  labeling any two adjacent lattice sites, and letting the phase,  $\phi_i \equiv \phi$ , be site-independent, but assuming any value in  $[0, 2\pi]$ , led to the following normal state Hamiltonian in RAFT [1,6,7]:

$$H \approx \sum_{\mathbf{k} \in \text{RBZ}} \Psi_{\mathbf{k}}^\dagger \mathcal{H} \Psi_{\mathbf{k}} + NUQ^2 - NU n^2 \quad (3)$$

where  $N$  is the number of sites and  $n = \langle n_{i,\sigma} \rangle$  is the expectation value of the number operator. Because of antiferromagnetic correlations, a bipartite lattice with sublattices  $A$  and  $B$  is considered, even though no long-range static antiferromagnetic order is taken into account. Note that RAFT is only valid away from half-filling, where this long-range order occurs. The summation runs over the reduced (magnetic) Brillouin zone (RBZ). The Nambu spinor is:  $\Psi_{\mathbf{k}}^\dagger = (c_{\mathbf{k}\uparrow}^{A\dagger} \ c_{\mathbf{k}\uparrow}^{B\dagger} \ c_{\mathbf{k}\downarrow}^{A\dagger} \ c_{\mathbf{k}\downarrow}^{B\dagger})$  and the Hamiltonian matrix is:

$$\mathcal{H} = \begin{pmatrix} -\mu' & \epsilon & UQe^{i\phi} & 0 \\ \epsilon & -\mu' & 0 & -UQe^{i\phi} \\ UQe^{-i\phi} & 0 & -\mu' & \epsilon \\ 0 & -UQe^{-i\phi} & \epsilon & -\mu' \end{pmatrix}$$

yielding the energy spectra:

$$E_{\pm}(\mathbf{k}) = -\mu'(\mathbf{k}) \pm E_q(\mathbf{k}) \quad (4)$$

where:  $\mu'(\mathbf{k}) = \mu - Un + 4t' \cos k_x \cos k_y$ ,  $E_q(\mathbf{k}) = \sqrt{\epsilon^2(\mathbf{k}) + (UQ)^2}$ , and  $\epsilon(\mathbf{k}) = -2t(\cos k_x + \cos k_y)$ . Using the fact that the energy spectra,  $E_{\pm}(\mathbf{k})$ , do not depend on phase  $\phi$ , the matrix,  $\mathcal{H}$ , is transformed to one that does not depend on  $\phi$  using the spin-dependent gauge transformation:  $c_{i,\uparrow} \rightarrow e^{i\phi/2} c_{i,\uparrow}$  and:

$c_{i,\downarrow} \rightarrow e^{-i\phi/2}c_{i,\downarrow}$ . This transformation is equivalent to performing a rotation by angle,  $-\phi$ , about the  $z$  axis for the  $x$  and  $y$  components of the spin operator according to:

$$\begin{pmatrix} S_i^x \\ S_i^y \end{pmatrix} \rightarrow \begin{pmatrix} \cos \phi & \sin \phi \\ -\sin \phi & \cos \phi \end{pmatrix} \begin{pmatrix} S_i^x \\ S_i^y \end{pmatrix}$$

Note that the thermal averages of  $S_i^x$  and  $S_i^y$  are given by:

$$\begin{aligned} \frac{\langle S_i^x \rangle}{\hbar} &= Q \cos \phi, \quad \frac{\langle S_i^y \rangle}{\hbar} = -Q \sin \phi, \quad i \in A, \text{ or} \\ \frac{\langle S_i^x \rangle}{\hbar} &= -Q \cos \phi, \quad \frac{\langle S_i^y \rangle}{\hbar} = Q \sin \phi, \quad i \in B \end{aligned} \quad (5)$$

and  $\langle S_i^z \rangle = 0$  for  $i$  in both sublattices. Because the phase,  $\phi$ , assumes any value between 0 and  $2\pi$ , rotational symmetry will not look broken for times greater than the period of rotation, as we will explain below, when we review the calculation of the time dependence of the phase. However, if the typical time scale of a probe is much smaller than this period, then symmetry may appear broken.

The magnitude,  $Q$ , and the electron occupation thermal average,  $n$ , are calculated by minimizing the phase-independent mean-field free energy. The following mean-field equations were obtained in the normal state [1,6,7]:

$$\begin{aligned} n &= \frac{1}{2N} \sum_{\mathbf{k}} \{n_F[E_+(\mathbf{k})] + n_F[E_-(\mathbf{k})]\} \\ Q &= \frac{U}{2N} \sum_{\mathbf{k}} \frac{n_F[E_-(\mathbf{k})] - n_F[E_+(\mathbf{k})]}{E_q(\mathbf{k})} \end{aligned} \quad (6)$$

where  $n_F$  is the Fermi-Dirac factor.

## 2.2. Calculation of the Time Dependence of the Phase

The nature of RAF has recently been completely understood after the phase,  $\phi$ , of its order parameter was calculated as a function of time [10]. Here, we summarize how this was done. The Heisenberg equation,  $\frac{dS_j^+}{d\tau} = \frac{1}{i\hbar}[S_j^+, H]$ , was calculated in the limit where electron hopping is neglected in comparison to  $\frac{U}{2}(S_j^+S_j^- + S_j^-S_j^+)$ . The values considered in RAFT for onsite Coulomb repulsion are in the range  $U \sim 3t-5t$ ; this is an intermediate coupling regime where  $U > t$ , but smaller than the bandwidth,  $\sim 8t$  when  $t' \ll t$ . Neglecting the effect of electron hopping energies in the Heisenberg equation can be justified on the grounds that spin dynamics are faster than charge dynamics. An onsite spin flip fluctuation needs a time,  $\tau \sim \hbar/U$ , to be realized, while a fluctuation caused by a charge hopping between adjacent sites takes a longer time,  $\tau \sim \hbar/t$ , ( $U > t$ ). In the Heisenberg equation, the bare original interaction was used instead of RAFT's Hamiltonian (3) in order to treat quantum fluctuations as best as possible. In this approximation, the following time equation was obtained [10]:

$$\frac{dS_j^+}{d\tau} \approx i\frac{U}{\hbar}S_j^+, \quad (\tau \text{ is time}) \quad (7)$$

in the intermediate regime where spin dynamics is not governed by the Heisenberg exchange coupling,  $4t^2/U$ . Note that the latter is suitable in the strong coupling limit ( $U/t \gg 1$ ) for the Hubbard model,

whereas RAFT is valid in the intermediate coupling regime. Integration over time,  $\tau$ , in Equation (7) gives the thermal average:

$$\langle S_j^+(\tau) \rangle \approx \langle S_j^+(0) \rangle e^{iU\tau/\hbar} \quad (8)$$

The phase can thus be written as  $\phi = U\tau/\hbar$  modulo  $2\pi$ , when  $\langle S_j^+(0) \rangle$  is identified with  $|\langle S_j^+(\tau) \rangle|$ ,  $(-\langle S_j^+(\tau) \rangle)$ , for sublattice  $A$ ,  $(B)$ , and  $e^{i\phi}$  with  $e^{iU\tau/\hbar}$ . Using this result, the magnetic configuration (5) is rewritten as follows:  $\langle S_i^x \rangle/\hbar = Q \cos(\omega_{sf}\tau)$ ,  $\langle S_i^y \rangle/\hbar = -Q \sin(\omega_{sf}\tau)$  for  $i$  in sublattice  $A$  or  $\langle S_i^x \rangle/\hbar = -Q \cos(\omega_{sf}\tau)$ ,  $\langle S_i^y \rangle/\hbar = Q \sin(\omega_{sf}\tau)$  for  $i$  in sublattice  $B$ , and  $\langle S_i^z \rangle = 0$  for  $i$  in sublattice  $A$  or  $B$ . These thermal averages describe a rotational motion for the spin components with angular frequency,  $\omega_{sf} = U/\hbar$ . The period,  $T_{sf} = 2\pi\hbar/U$ , is thus the time required to perform a spin-flip process or the time needed for the rotating order parameter,  $\langle S_i^{x(y)} \rangle$ , to complete a  $2\pi$ -revolution in a classical picture.

### 2.3. Interpretation of Rotating Antiferromagnetism

The above derivation of RAF was supported by the following argument, which shows that rotating magnetism (ferro or antiferro) is physically sound and can therefore be realized in a real system independently of a model. Consider the much simpler case of a single spin precessing in a magnetic field,  $B$ , along the  $z$ -axis, with the initial spin state given by:  $|S_x, +\rangle = \frac{1}{\sqrt{2}}(|\uparrow\rangle + |\downarrow\rangle)$ . Initially, this spin points in the positive  $x$ -direction. The time-dependent expectation values of this spin's components are  $\langle S^x \rangle = \frac{\hbar}{2} \cos(\omega t)$ ,  $\langle S^y \rangle = \frac{\hbar}{2} \sin(\omega t)$ , and  $\langle S^z \rangle = 0$ , with  $\omega = \frac{|e|B}{m_e c}$ .  $e$  and  $m_e$  are the charge and mass of the electron, and  $c$  is the speed of light. The  $x$  and  $y$  components are therefore confined to rotate about the  $z$ -axis in the  $xy$  plane with Larmor angular frequency  $\omega$ . A rotating ferromagnetic state can be realized by placing  $N$  such states with the same frequency on a lattice made of  $N$  sites. For a rotating antiferromagnetic state, opposite initial states ( $\pm|S_x, +\rangle$ ) where spins point in opposite directions on the  $x$ -axis are placed on any two adjacent sites of a lattice. To relate RAF to spin flip processes, it is noted that  $\langle S^\pm \rangle = \langle S^x \rangle \pm i\langle S^y \rangle = \frac{\hbar}{2} e^{\pm i\omega t}$  in this example. In a given model, a coupling is necessary for providing the building blocks for RAF, which is a spin precessing about an effective magnetic field (with no local magnetization) for each lattice site and the anti-alignment of the adjacent rotating moments. The RAF state constructed in this way shows a hidden order that can be realized even at finite temperature without violating the Mermin-Wagner theorem [11].

The above simple case allowed us to interpret RAF as a state where spins precess collectively in a synchronized way in the spins'  $xy$  plane around a staggered effective magnetic field,  $B = m_e c U/\hbar |e|$ , generated by onsite Coulomb repulsion.  $\hbar/2$  in  $\langle S^\pm \rangle = \frac{\hbar}{2} e^{\pm i\omega t}$  is replaced by the magnitude of the RAF order parameter,  $Q\hbar$ , which assumes values smaller than  $\hbar/2$ , due to thermal fluctuations. In comparison to ordinary spin waves in an antiferromagnet, RAF's state was interpreted as a single  $\mathbf{q} = (\pi, \pi)$  spin wave occurring as a consequence of zero staggered static magnetization. The spin-wave theory does not, however, apply for our system (where  $\langle S_i^z \rangle = 0$ ), since this theory has to be built on top of a Néel background with finite  $\langle S_i^z \rangle$ . Also, in comparison to the ordinary antiferromagnetic spin-density order, RAF is characterized by a local magnetization that is not static, because of the time dependence of the phase of the magnetization. It is thus clear that RAF will have all the typical effects of spin-density order on the evolution of the electronic structure with doping, but is expected to go undetected for

experimental probes, like neutrons, due to the time dependence of the phase. We predicted [10] that rotational symmetry will not look broken for experimental probes that are characterized by a time scale greater than the period of rotation  $T_{sf} = 2\pi\hbar/U$  of the rotating order parameter of RAF. For such probes, averaging over times longer than the period will not allow for the observation of RAF. In RAFT, electron hopping energy,  $t$ , is taken to be 0.1 eV when fitting data. Taking  $U = 3t = 0.3$  eV gives  $T_{sf} \approx 10^{-14}$  s. For neutrons, for example, the typical time would be the time spent by a given neutron in the immediate vicinity of a given spin during the scattering process. If this time is greater than the period,  $T_{sf}$ , then neutrons will not detect RAF. If the time spent by the neutron in the vicinity of the spin is smaller, then there is a chance RAF will be detected. Note that smaller times mean higher energies for neutrons. This is an issue that is still under investigation and will be reported on in the future.

#### 2.4. Interplay between RAF and SC

In RAFT, d-wave SC was introduced phenomenologically using an attractive coupling between electrons on adjacent sites. The term,  $-V \sum_{\langle i,j \rangle} n_{i,\uparrow} n_{j,\downarrow}$ , is now added to Hamiltonian (1) and is decoupled using  $D_{\langle i,j \rangle} = \langle c_{i,\downarrow} c_{j,\uparrow} \rangle$ . To get a d-wave gap, we set  $D_{\langle i,j \rangle} = D_0$  along the  $x$ -direction and  $D_{\langle i,j \rangle} = -D_0$  along the  $y$ -direction [1,6].

When both SC and RAF orders are taken into account, the mean-field Hamiltonian is written in terms of an eight-component spinor, given by:

$$\Psi_{\mathbf{k}}^{\dagger} = (c_{-\mathbf{k}\uparrow}^{A\dagger} c_{-\mathbf{k}\uparrow}^{B\dagger} c_{\mathbf{k}\downarrow}^A c_{\mathbf{k}\downarrow}^B c_{\mathbf{k}\uparrow}^A c_{\mathbf{k}\uparrow}^B c_{-\mathbf{k}\downarrow}^{A\dagger} c_{-\mathbf{k}\downarrow}^{B\dagger}) \quad (9)$$

and assumes the expression [1,6]:

$$H = \sum_{\mathbf{k} <} \Psi_{\mathbf{k}}^{\dagger} \mathcal{H} \Psi_{\mathbf{k}} + UNQ^2 + UNm^2 + 4VND_0^2 - UNn^2 - \mu N \quad (10)$$

where  $\mathcal{H}$  is an  $8 \times 8$  matrix:

$$\mathcal{H} = \begin{pmatrix} \mathcal{H}' & \mathcal{U}_Q \\ -\mathcal{U}_Q & -\mathcal{H}' \end{pmatrix}$$

with  $\mathcal{H}'$  and  $\mathcal{U}_Q$ , two  $4 \times 4$  matrices, given by:

$$\mathcal{H}' = \begin{pmatrix} -\mu'(\mathbf{k}) & \epsilon(\mathbf{k}) & 0 & D(\mathbf{k}) \\ \epsilon(\mathbf{k}) & -\mu'(\mathbf{k}) & D(\mathbf{k}) & 0 \\ 0 & D(\mathbf{k}) & \mu'(\mathbf{k}) & -\epsilon(\mathbf{k}) \\ D(\mathbf{k}) & 0 & -\epsilon(\mathbf{k}) & \mu'(\mathbf{k}) \end{pmatrix}$$

and:

$$\mathcal{U}_Q = \begin{pmatrix} 0 & 0 & QU & 0 \\ 0 & 0 & 0 & -QU \\ -QU & 0 & 0 & 0 \\ 0 & QU & 0 & 0 \end{pmatrix}$$

The  $\mathbf{k}$ -dependent superconducting gap is  $D(\mathbf{k}) = 2VD_0(\cos k_x - \cos k_y)$ , where  $D_0 = \langle c_{2i,j,\downarrow}^A c_{2i\pm 1,j\uparrow}^B \rangle = -\langle c_{i,2j,\downarrow}^A c_{i,2j\pm 1,\uparrow}^B \rangle$  involves two adjacent sites on different sublattices. Triplet SC [12] is ruled out by

choosing  $\langle c_{2i,j,\downarrow}^A c_{2i\pm 1,j,\uparrow}^B \rangle = -\langle c_{2i,j,\uparrow}^A c_{2i\pm 1,j,\downarrow}^B \rangle$ ; so, only spin-singlet SC, which is relevant to HTSCs, is considered in RAFT. The way decoupling is done using creation and annihilation operators rather than the spin-singlet and triplet superconducting operators, which are a combination of products of the  $c$ 's and  $c^\dagger$ 's, allowed us to avoid the generation of triplet SC if it is not present initially [12].

In Hamiltonian (10),  $\epsilon(\mathbf{k}) = -2t(\cos k_x + \cos k_y)$ , and  $\mu'(\mathbf{k}) = \mu - Un + 4t' \cos k_x \cos k_y$  have the same expressions as in the absence of SC. In Equation (10), the summation over  $\mathbf{k}$  takes into account the doubling of the Brillouin zone and the fact that summation is now over  $\mathbf{k}$  and  $-\mathbf{k}$ . The size of the mean-field Hamiltonian matrix,  $\mathcal{H}$ , is twice as large as that in the density  $d$ -wave (DDW) approach [13], proposed for the PG behavior, or in other approaches that deal with the interplay between antiferromagnetism and SC [12].

The energy spectra obtained by diagonalizing the matrix  $\mathcal{H}$  are  $\pm E_1(\mathbf{k})$  and  $\pm E_2(\mathbf{k})$  with:

$$E_\nu(\mathbf{k}) = \sqrt{[\mu'(\mathbf{k}) + (-1)^\nu E_q(\mathbf{k})]^2 + D^2(\mathbf{k})}, \quad \nu = 1, 2 \quad (11)$$

where:  $E_q(\mathbf{k}) = \sqrt{\epsilon^2(\mathbf{k}) + Q^2 U^2}$ .

Minimizing the free energy function with respect to  $Q$  and  $D_0$ , and calculating the density of electrons,  $n$ , led to the following mean-field equations that describe the interplay between RAF and SC for HTSCs with tetragonal symmetry:

$$\begin{aligned} 1 &= \frac{V}{4N} \sum_{\mathbf{k}, \nu=1,2} \frac{(\cos k_x - \cos k_y)^2}{E_\nu} \tanh\left(\frac{\beta E_\nu}{2}\right) \\ 1 &= \frac{U}{4N} \sum_{\mathbf{k}, \nu=1,2} (-1)^{\nu+1} \frac{A_\nu}{E_q} \tanh\left(\frac{\beta E_\nu}{2}\right) \\ n &= -\frac{1}{4N} \sum_{\mathbf{k}, \nu=1,2} A_\nu \tanh\left(\frac{\beta E_\nu}{2}\right) + \frac{1}{2} \end{aligned} \quad (12)$$

where:

$$A_\nu(\mathbf{k}) = [-\mu'(\mathbf{k}) - (-1)^\nu E_q(\mathbf{k})]/E_\nu(\mathbf{k}) \quad (13)$$

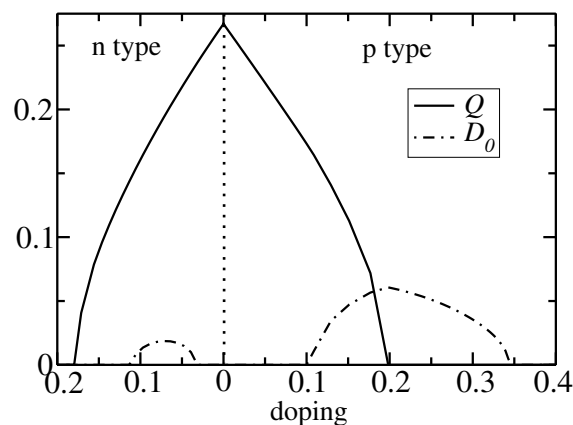
In the case of crystals with orthorhombic symmetry, it is possible that  $D_{\langle i,j \rangle_x} \neq -D_{\langle i,j \rangle_y}$ , because the superconducting coupling constants,  $V_x$ , along the  $x$  axis and,  $V_y$ , along the  $y$  axis, may differ. Then, the superconducting gap takes on the form:  $D(\mathbf{k}) = \psi_s(\cos k_x + \cos k_y) + \psi_d(\cos k_x - \cos k_y)$  with  $\psi_s = V_x D_x - V_y D_y$  and  $\psi_d = V_x D_x + V_y D_y$ , which implies that it shows  $d+s$ -pairing symmetry. This is a consequence of the absence of invariance under rotations by  $\pi/2$  of the  $\text{CuO}_2$  plane and is therefore consistent with arguments based on group theory [14].

### 3. RAF and SC Parameters versus Temperature and Doping

The mean-field Equations (12) were solved numerically in order to get the parameters,  $Q$ ,  $D_0$ , and the average number of electrons per site and per spin,  $n$ . In hole-doped (p-type) systems, the density of holes given by  $p = 1 - 2n$  is equivalent to the density of electrons missing below half-filling. For electron-doped (n-type) systems, the density of electrons  $n_e = 2n - 1$  is the density of electrons above half-filling. Note that at half-filling,  $n = 1/2$ , so that  $n_e = p = 0$  in this case.

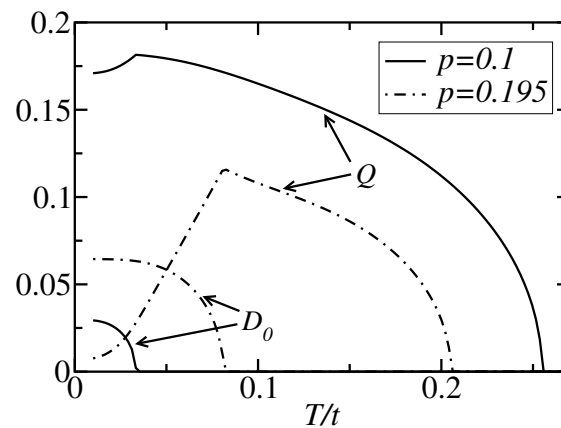
Figure 1 shows RAF and SC parameters,  $Q$  and  $D_0$ , versus doping for the Hamiltonian parameters,  $U = 2.8t$ ,  $V = 0.85t$  and  $t' = -0.16t$ . If RAF were not taken into account, SC would be optimum at half-filling. When RAF is allowed in, SC is destroyed near half-filling, but coexists with RAF in the underdoped regime for p-type doping and for all doping values where  $D_0 \neq 0$  in n-type case. The doping values where  $Q$  vanishes in both p- and n-type systems are identified as quantum critical points (QCP) [1]. In Figure 1, the QCP occurs within the superconducting dome in the p-type system, but outside of the dome and deep in the overdoped regime for the n-type system. RAF's parameter,  $Q$ , has been proposed to model the PG in HTSCs [1,6], and the PG temperature  $T^*$  has been identified with the temperature below which  $Q$  becomes nonzero.

**Figure 1.** The typical behavior of the rotating order parameter,  $Q$ , and superconducting parameter,  $D_0$ , with doping is illustrated here for  $U = 2.8t$ ,  $V = 0.85t$  and  $t' = -0.16t$ . Temperature is  $T = 0.05t$ . The behavior shown is practically the same at zero temperature. The doping values where  $Q$  vanishes in both p- and n-type cases are interpreted as quantum critical points (QCP).



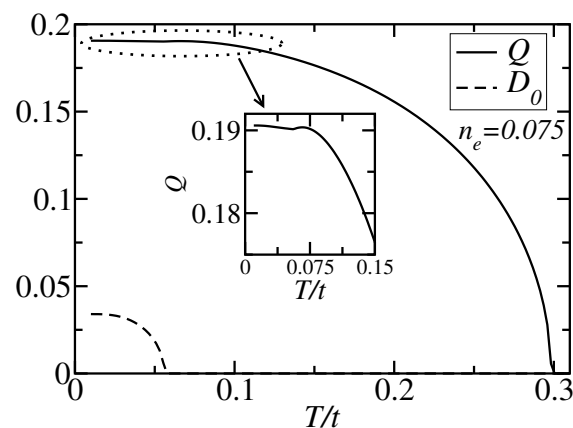
Figures 2 and 3 display the temperature dependence for  $Q$  and  $D_0$  for some given doping levels. Using these kind of figures, the PG ( $T^*$ ) and SC ( $T_C$ ) temperatures were calculated in [6] for p-type cuprates. Again, the competition is apparent between SC and RAF in the p-type case, because as soon as  $D_0$  becomes nonzero, RAF's order parameter,  $Q$ , decreases monotonically, as seen in Figure 2 for  $p = 0.1$  in the underdoped regime. Note that the optimal doping for the Hamiltonian parameters used here is  $p \approx 0.20$  in the p-type case and  $n_e \approx 0.075$  in the n-type case; see Figure 1. For  $p = 0.195$  (close to optimal doping), it is interesting to note that  $Q$  decreases significantly below  $T_C$  when  $D_0$  becomes nonzero. The behavior for n-type case is totally different. For  $n_e = 0.075$  (optimal doping),  $Q$  barely decreases when  $D_0$  becomes nonzero below  $T_C$ , then even increases slightly and saturates at low temperature, as the inset of Figure 3 shows.

**Figure 2.** The temperature dependence of  $Q$  and  $D_0$  is displayed for two values of doping in the p-type case. The Hamiltonian parameters are  $U = 2.8t$ ,  $V = 0.85t$  and  $t' = -0.16t$ .



The phase diagram obtained by letting in a Bardeen-Cooper-Schrieffer [15] picture  $T^* \sim Q(T = 0)$  and  $T_C \sim D_0(T = 0)$  in Figure 1 is in qualitative agreement with experiments for p-type  $\text{La}_{2-x}\text{Sr}_x\text{CuO}_4$  and n-type  $\text{Nd}_{2-x}\text{Ce}_x\text{CuO}_4$  cuprates. For the latter, the PG is reported to vanish almost when SC does in the overdoped regime [2]. For the former, significant experimental evidence suggests the disappearance of the PG rather closer to the optimal doping [16].

**Figure 3.** The temperature dependence of  $Q$  and  $D_0$  is displayed for an n-type case with  $n_e = 0.075$ . The Hamiltonian parameters used are  $U = 2.8t$ ,  $V = 0.85t$  and  $t' = -0.16t$ .



In RAFT, the thermal average of the spin operators,  $S_i^x$  and  $S_i^y$ , in a frame rotating with angular frequency,  $\omega_{sf}$ , with the rotating local magnetization are  $\langle S_i^x \rangle = (\langle S_i^+ \rangle + \langle S_i^- \rangle)/2 = (-1)^{x_i+y_i}|Q|$ , and  $\langle S_i^y \rangle = 0$ , respectively, and by construction, the static magnetization along the quantization axis,  $z$ , is zero in order to satisfy the Mermin-Wagner theorem at finite temperature. Here,  $x_i$  and  $y_i$  are the  $x$  and  $y$  coordinates of site,  $i$ . RAF is predicted to exist in a purely two-dimensional electronic system or in a three-dimensional system of electrons, where either thermal fluctuations at high temperature or doping even at lower temperature prevents three-dimensional long-range Néel order from occurring. Néel order, which has not been taken into account so far in RAFT, occurs below  $T_N < T^*$  in the vicinity of half-filling. As is well known, this antiferromagnetic phase consists of a static magnetization plus quantum spin waves, which exist for all allowed wavevectors. How then does RAF evolve into static

antiferromagnetism when temperature is lowered below  $T_N$  for a given doping density, and how does static antiferromagnetism give way to the pseudogap phase when doping increases away from half-filling at a given temperature? The key point in answering these questions may perhaps reside in the fact that RAF has been interpreted as a single  $q = (\pi, \pi)$  wave [10]. We conjecture that when temperature is lowered across  $T_N$ , the static magnetization sets in, due to the three-dimensional coupling between the copper-oxygen layers. The establishment of three-dimensional long-range order naturally allows other spin waves with  $q \neq (\pi, \pi)$  to settle in along with the  $q = (\pi, \pi)$  spin wave present in RAF, a mechanism that causes the loss of RAF. In this conjecture, the PG is a consequence of purely two-dimensional physics, but the Néel order is, as is well known due to three-dimensional physics. In future investigations, we plan to seek the mechanism for the phase change from the Néel order to RAF and *vice versa*.

## 4. Doping Dependence of Electronic Structure

### 4.1. Analysis of Energy Spectra

As mentioned in the previous section, the appearance of RAF below a critical value of doping as the latter is reduced from the overdoped to underdoped regime for p-type or n-type systems at zero temperature has been interpreted as a QCP. The case of p-type has been discussed before [1,6,8]. This QCP induces a reconstruction of the FS practically in the same way an ordinary spin-density order does [17]. However, RAF is not an ordinary spin density order, as explained in Section 2. Figure 4 shows energy spectra along symmetry lines of the Brillouin zone for  $T = 0.1t$ . For  $p = 0.075$ , one clearly sees a gap at  $(\pi, 0)$ , in agreement with experimental data for  $\text{La}_{2-x}\text{Sr}_x\text{CuO}_4$  [18]. Also a small hole-like band is seen along the diagonal around  $(\pi/2, \pi/2)$ . The presence of the gap at  $(\pi, 0)$  for this doping and the small hole-like band in the vicinity of  $(\pi/2, \pi/2)$  are due to the nonzero value of RAF's order parameter,  $Q$ . This gap is responsible for the PG behavior in the underdoped regime. The hole-like band is also seen along the RBZ boundary  $[(\pi, 0) \rightarrow (0, \pi)]$ , as shown in Figure 5 for  $p = 0.1$ . For  $p = 0.24$  in the overdoped regime, the PG has closed, and the hole-like pocket has reached the  $(\pi, 0)$  and  $(0, \pi)$  points, as can be seen along the RBZ boundary in Figure 5. Along this boundary,  $E_+(\mathbf{k}) = E_-(\mathbf{k})$ , when  $Q = 0$  at  $T = 0.1t$ , is above the chemical potential all the way between  $(\pi, 0)$  and  $(0, \pi)$ .

For the n-type case, Figure 6 displays the spectra for doping  $n_e = 0.06$  in the underdoped regime and for  $n_e = 0.2$  well in the overdoped regime for  $T = 0.1t$ . The PG behavior is now a consequence of a gap at  $(\pi/2, \pi/2)$ , and a small electron pocket forms near  $(\pi, 0)$ . For  $n_e = 0.2$ , the PG is zero, because  $Q$  has vanished, and the electron pocket at  $(\pi, 0)$  joined that at  $(0, \pi)$ . This can be understood by examining the spectrum along the RBZ boundary, which gives a completely full band along this direction. For example, for  $n_e = 0.21$  in Figure 5,  $E_+(\mathbf{k}) = E_-(\mathbf{k}) < 0$ , which means that these bands are full. The above analysis can be made even more transparent by calculating the FS, a task undertaken below.

**Figure 4.** The energies  $E_-(\mathbf{k})$  and  $E_+(\mathbf{k})$  are plotted versus  $\mathbf{k}$  along symmetry lines of the Brillouin zone. The Hamiltonian parameters are  $U = 2.8t$ ,  $V = 0.85t$  and  $t' = -0.16t$ , and hole doping is  $p = 0.075$  in the underdoped phase for the figure on the left and  $p = 0.24$  in the overdoped regime for the figure on the right. The dotted horizontal line indicates the position of the Fermi energy. Temperature is  $T = 0.1t$  and  $D_0 = 0$ .

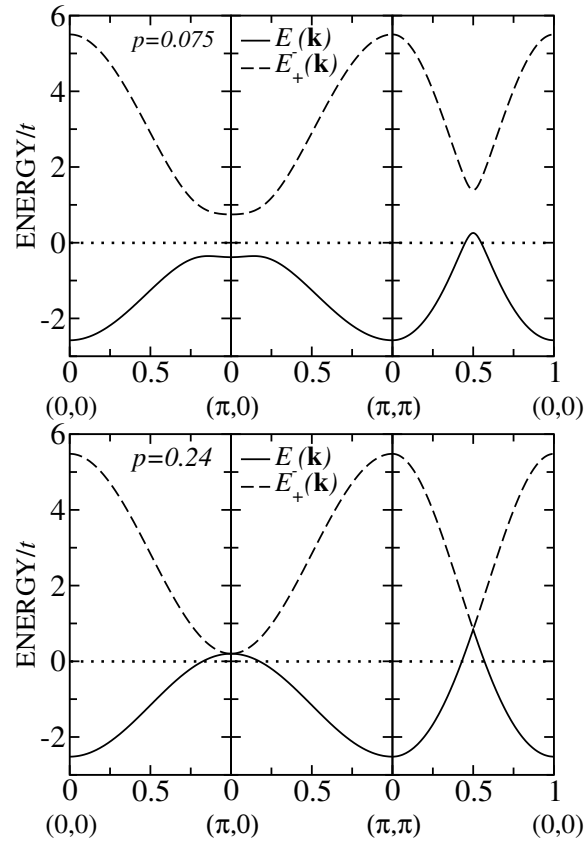


**Figure 5.** The energy spectra along the boundary of the magnetic Brillouin zone  $((\pi, 0) \rightarrow (0, \pi))$  is shown. Temperature is  $T = 0.1t$  and  $D_0 = 0$ .

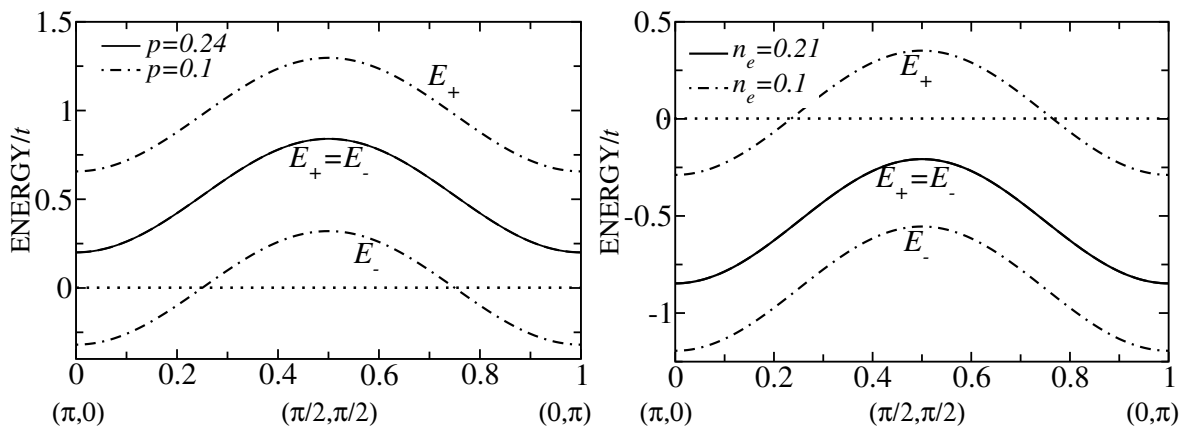
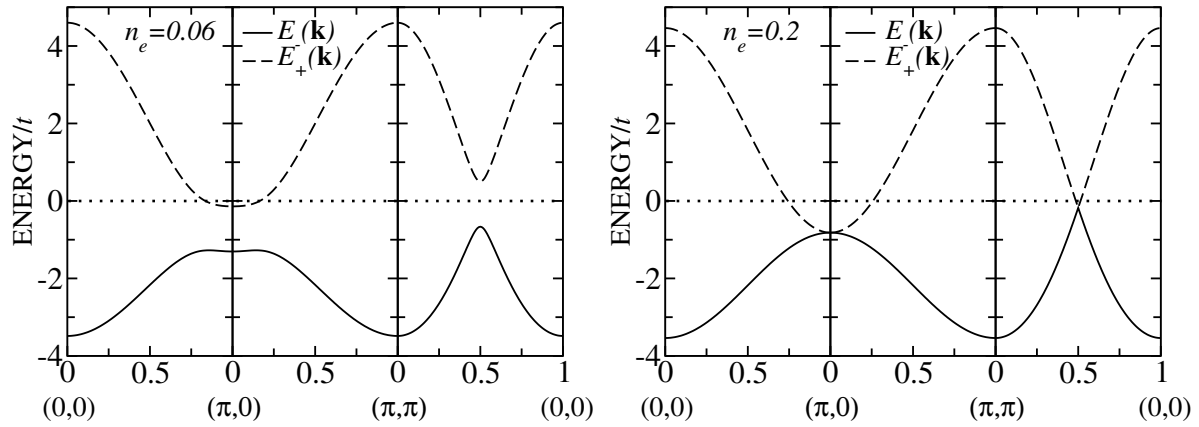


**Figure 6.** The energies  $E_-(\mathbf{k})$  and  $E_+(\mathbf{k})$  are plotted versus  $\mathbf{k}$  along symmetry lines of the Brillouin zone. The Hamiltonian parameters are  $U = 2.8t$ ,  $V = 0.85t$  and  $t' = -0.16t$ , and electron doping is  $n_e = 0.06$  in the underdoped phase for the figure on the left and  $n_e = 0.2$  in the overdoped regime for the figure on the right. Temperature is  $T = 0.1t$  and  $D_0 = 0$ .



#### 4.2. Evolution of the Fermi Surface with Doping

In RAFT, the occupation probability,  $n(\mathbf{k})$ , was defined by writing the average number of electron per spin and site  $n$  in Equation (12) as:  $n \equiv \frac{1}{N} \sum_{\mathbf{k}} n(\mathbf{k})$ , which yields [1]:

$$n(\mathbf{k}) = -\frac{1}{4} \sum_{\nu=1,2} A_{\nu}(\mathbf{k}) \tanh\left[\frac{\beta E_{\nu}(\mathbf{k})}{2}\right] + \frac{1}{2} \quad (14)$$

$A_{\nu}(\mathbf{k})$  is given in Equation (13).  $n(\mathbf{k})$  was then interpreted as the probability that the state with wave vector,  $\mathbf{k}$ , is occupied by an electron with spin up or down.

Ronning *et al.* [19] extracted  $n(\mathbf{k})$  by integrating ARPES energy distribution curves over energy for the material,  $\text{Ca}_2\text{CuO}_2\text{Cl}_2$ , then deduced the FS by locating the steepest drops in  $n(\mathbf{k})$  in analogy with a Fermi gas. Also, using the same method, the Fermi surface for  $\text{Bi}_2\text{Sr}_2\text{CaCu}_2\text{O}_{8+\delta}$  in the overdoped regime was obtained. Here, we implement the same argument in RAFT, namely the FS is determined by the sharp drops in the occupation probability. This method was also used in [5] and gave results in agreement with the determination of the FS using the spectral function.

Figure 7 shows two-dimensional plots of  $n(\mathbf{k})$  for three doping levels in the p-type case for Hamiltonian parameters  $U = 2.8t$ ,  $V = 0.85t$  and  $t' = -0.16t$  at temperature  $T = 0.1t$ . This temperature is above any transition temperature for SC. The FS is made of hole pockets around  $(\pm\pi/2, \pm\pi/2)$  in the underdoped regime, as shown for  $p = 0.06$ . The energy spectra in Figures 4 and 5 show well that in the presence of the PG, the upper  $E_+$  and lower  $E_-$  bands are separated by gaps along all the symmetry lines in the underdoped regime. Hole-like pockets can clearly be seen for  $p = 0.075$  in Figure 4 around  $(\pi/2, \pi/2)$ . Around optimal doping,  $p = 0.2$ , the hole pockets reach the points,  $(\pm\pi, 0)$  and  $(0, \pm\pi)$ . In the overdoped regime, where the PG is zero, the FS is made of large contours around  $(0, 0)$  and  $(\pi, \pi)$ , as can be seen in Figure 4 for  $p = 0.24$ . For the latter, because the PG is zero, the upper band  $E_+$  and lower band  $E_-$  touch at  $(\pm\pi, 0)$ ,  $(0, \pm\pi)$  and  $(\pm\pi/2, \pi/2)$  to form a tight-binding spectrum given by  $E_{\pm}(\mathbf{k}) = \pm|2t(\cos k_x + \cos k_y)| - 4t' \cos k_x \cos k_y - \mu + Un$ . The presence of the absolute value

in this tight-binding energy is a consequence of the limit,  $Q \rightarrow 0$ , in  $\sqrt{\epsilon^2(\mathbf{k}) + U^2 Q^2}$  for the overdoped regime. In the p-type case, the FS in RAFT thus evolves strongly with doping. It reconstructs at the QCP doping, where  $Q$  vanishes. Its topology changes from small hole-like pockets in the underdoped regime below this QCP to large contours in the overdoped regime. This is qualitatively consistent with the quantum oscillations observed in resistivity by Doiron-Leyraud *et al.* [20] for  $\text{YBa}_2\text{Cu}_3\text{O}_{6.5}$ , which indicated that a well-defined small FS characterizes this underdoped cuprate. Subsequent work by Sebastian *et al.* [21] for  $\text{YBa}_2\text{Cu}_3\text{O}_{6+x}$  supported the existence of small closed pockets in the underdoped regime, as well.

The calculated FS undergoes also a significant reconstruction when doping changes from p-type to n-type across half-filling, (note that RAFT is only valid outside of the HTSCs' AF phase around half-filling). In RAFT, for the Hamiltonian parameters considered here, the FS in the underdoped regime for n-type cuprates consists of electron pockets around points  $(\pm\pi, 0)$  and  $(0, \pm\pi)$ , rather than pockets around  $(\pm\pi/2, \pm\pi/2)$  in the underdoped regime of p-type cuprates. This is clearly seen in Figure 8 for  $n_e = 0.06$  and  $n_e = 0.1$  and is consistent with the energy spectra in Figure 6, which show the existence of a small electron pocket at  $(\pi, 0)$  for  $n_e = 0.06$  as well. When the PG vanishes in the overdoped regime, the electron pockets join to form large contours, as seen for  $n_e = 0.2$ . Armitage *et al.* [3] reported ARPES data for n-type material  $\text{Nd}_{2-x}\text{Ce}_x\text{CuO}_4$ , which can be interpreted as revealing the existence of pockets around  $(\pi, 0)$  and symmetric points in the underdoped regime. Also, Matsui *et al.* [22] measured the evolution of the FS with doping for this material using ARPES. A close look at Figure 1 of their work reveals a FS mainly near  $\mathbf{k}$ -points  $(\pi, 0)$  and  $(0, \pi)$  for doping  $x = 0.13$ , but the FS evolves into larger contours joining these two points for the larger doping levels,  $x = 0.16$  and  $x = 0.17$ . Note that if one symmetrizes Matsui *et al.*'s FSs about the line joining  $(\pi, 0)$  and  $(0, \pi)$ , one will get FSs that look similar to those calculated here and shown in Figure 8. Their measurements were done only along the FS in the tight-binding limit. We predict that if measurements were performed along the image of this tight-binding FS with respect to line  $(\pi, 0)$ - $(0, \pi)$ , then one would obtain a FS that looks like ours. Also, the reconstruction of the FS, as illustrated in Figure 8, at the QCP doping, where  $Q$  vanishes (so, where the PG vanishes), is in agreement with the SdH oscillation results of Helm *et al.* [2] for the above material. SdH oscillations revealed a FS evolving from small pockets to large contours as doping goes from the underdoped regime to overdoped regime.

## 5. Conclusions and Discussion

We studied the reconstruction of the Fermi surface under the effect of the hidden rotating antiferromagnetic order in both p-type and n-type high- $T_C$  cuprates. For the Hamiltonian parameters used here, the Fermi surface in p-type cuprates reconstructs, due to rotating antiferromagnetism at the quantum critical point near optimal doping, where the pseudogap vanishes. This Fermi surface consists of hole pockets around  $(\pm\pi/2, \pm\pi/2)$  in the underdoped regime, but changes to large closed contours in the overdoped regime. For n-type cuprates, the location and topology of the Fermi surface is different than in p-type materials. The hole pockets are of a form resembling squares around  $(\pm\pi, 0)$  and  $(0, \pm\pi)$  in deep underdoped n-type systems. When the pseudogap becomes zero beyond the quantum critical point in the overdoped regime, the Fermi surface changes to large closed contours. These results are in

good qualitative agreement with experimental data for  $\text{La}_{2-x}\text{Sr}_x\text{CuO}_4$  and  $\text{Nd}_{2-x}\text{Ce}_x\text{CuO}_4$  for the set of Hamiltonian parameters used in the present calculations.

**Figure 7.** The occupation probability,  $n(\mathbf{k})$ , is shown in the Brillouin zone. The hole densities are shown on the graphs. The Hamiltonian parameters are  $U = 2.8t$ ,  $V = 0.85t$ , and  $t' = -0.16t$  and  $T = 0.1t$ .

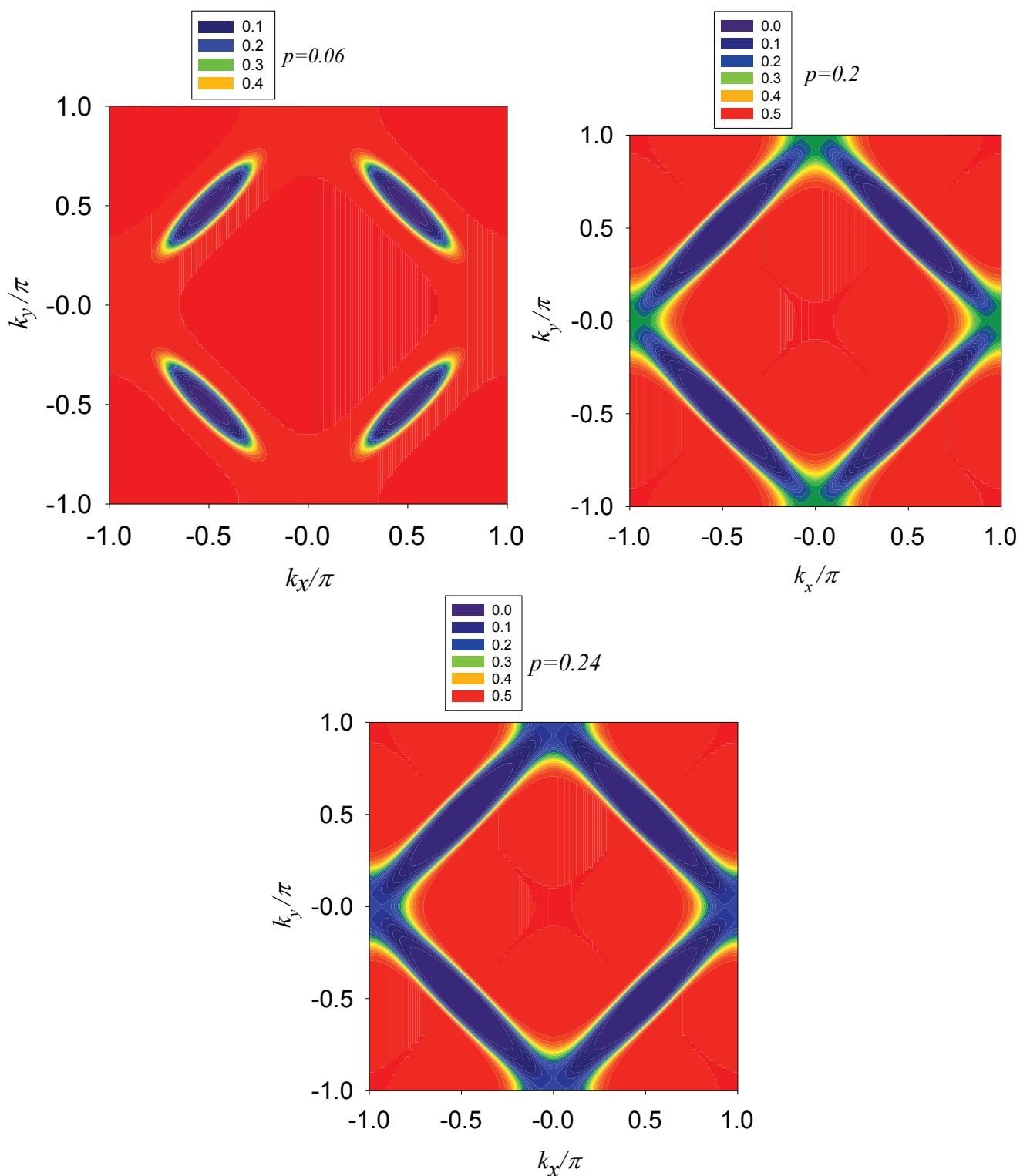
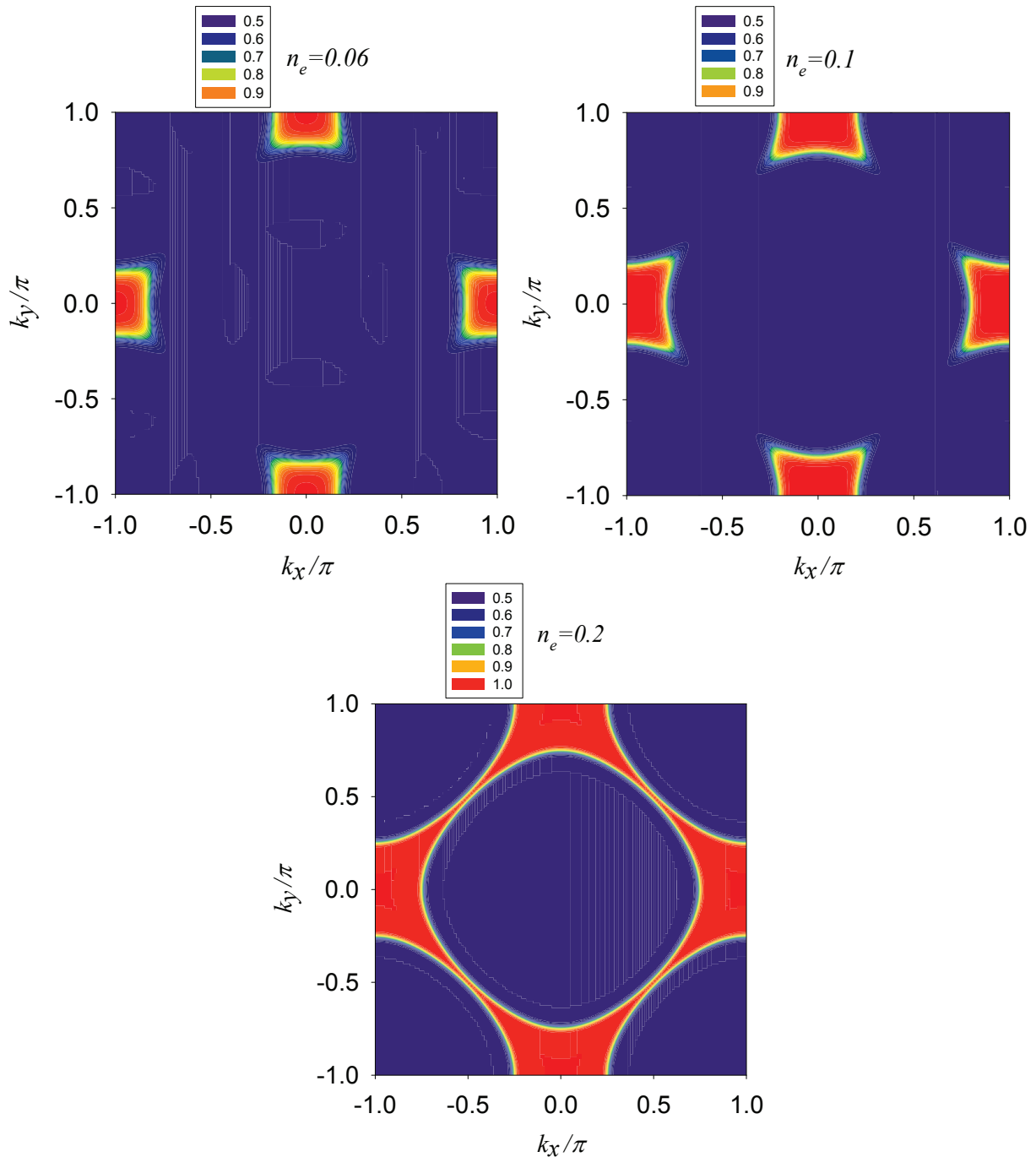


**Figure 8.** The occupation probability,  $n(\mathbf{k})$ , is shown in the Brillouin zone. The electron densities above half-filling,  $n_e$ , are shown on the graphs. The Hamiltonian parameters are  $U = 2.8t$ ,  $V = 0.85t$  and  $t' = -0.16t$ , and temperature is  $T = 0.1t$ .



The issue of the applicability of the rotating antiferromagnetism theory for the high- $T_C$  materials ought to be discussed in the context of other experimental results. For example, one needs to analyze in this theory the unusual antiferromagnetic order observed using polarized neutron scattering by Fauqué *et al.* [23] in  $\text{YBa}_2\text{C}_3\text{O}_{6+\delta}$ , and by Li *et al.* [24] in  $\text{HgBa}_2\text{CuO}_{4+\delta}$ . These polarized neutron measurements probed the spin-flip response. While it is not yet clear how to interpret these measurements in the framework of RAFT, it is interesting to note that rotating antiferromagnetism is

also based on the spin-flip processes in the Hubbard model [1,6]. So, could the occurrence of long-range coherence for these spin flip processes, as discussed in [10], yield a magnetic signal identical to that observed using polarized neutrons? This question needs to be addressed both experimentally and theoretically. One also needs to reconcile the rotating antiferromagnetism theory with other observed types of orders, like the charge-density wave order observed by Chang *et al.* [25], found using x-ray diffraction, and with the observation by Shekhter *et al.* [26] of a second-order phase transition in resonant ultrasound spectroscopy. The charge-density wave order has been observed well below the pseudogap temperature,  $T^*$ ; it can thus not be claimed to be responsible for the pseudogap state in any way, and such an order is not included in RAFT. Regarding the observation at  $T^*$  of a second-order phase transition in resonant ultrasound spectroscopy, we stress that even though RAF is a dynamic order, the rotating order parameter has a magnitude that behaves as in a second-order phase transition [1,6], thus in qualitative agreement with this experimental finding. Finally, Dean *et al.* [27] reported spin-wave(magnon)-like excitations in a single layer  $\text{La}_2\text{CuO}_4$  that resemble the magnon excitations observed in the bulk material,  $\text{La}_2\text{CuO}_4$ . As the long-range antiferromagnetic order is ruled out in a single layer at finite temperature, due to thermal spin fluctuations, one needs to find an explanation for this result outside of the linear spin-wave theory. Also, Dean *et al.* ruled out the possibility of interpreting their finding within the resonating-valence bond theory. The question that naturally arises is whether fluctuations beyond the mean-field point in the rotating antiferromagnetism theory can mimic this observed magnon-like dispersion. The calculation of the dispersion due to such fluctuations is underway and will be reported on in the future.

## References

1. Azzouz, M. Rotating antiferromagnetism in high-temperature superconductors. *Phys. Rev. B* **2003**, *67*, 134510:1–134510:12.
2. Helm, T.; Kartsovnik, M.V.; Bartkowiak, M.; Bittner, N.; Lambacher, M.; Erb, A.; Wosnitza, J.; Gross, R. Evolution of the fermi surface of the electron-doped high-temperature superconductor  $\text{Nd}_{2-x}\text{Ce}_x\text{CuO}_4$  Revealed by Shubnikov–de Haas Oscillations. *Phys. Rev. Lett.* **2009**, *103*, 157002:1–157002:4.
3. Armitage, N.P.; Ronning, F.; Lu, D.H.; Kim, C.; Damascelli, A.; Shen, K.M.; Feng, D.L.; Eisaki, H.; Shen, Z.-X.; Mang, P.K.; *et al.* Doping dependence of an n-type cuprate superconductor investigated by angle-resolved photoemission spectroscopy. *Phys. Rev. Lett.* **2002**, *88*, 257001:1–257001:4.
4. Yoshida, T.; Zhou, X.J.; Tanaka, K.; Yang, W.L.; Hussain, Z.; Shen, Z.-X.; Fujimori, A.; Sahrakorpi, S.; Lindroos, M.; Markiewicz, R.S.; Bansil, A.; *et al.* Systematic doping evolution of the underlying Fermi surface of  $\text{La}_{2-x}\text{Sr}_x\text{CuO}_4$ . *Phys. Rev. B* **2006**, *74*, 224510:1–224510:5.
5. Azzouz, M.; Ramakko, B.W.; Presenza-Pitman, G. The electronic structure of the high- $T_C$  cuprates within the hidden rotating order. *J. Phys. Condens. Matter* **2010**, *22*, 345605:1–345605:15.
6. Azzouz, M. Thermodynamics of high- $T_C$  materials in the rotating antiferromagnetism theory. *Phys. Rev. B* **2003**, *68*, 174523:1–174523:12.
7. Azzouz, M. Chemical potentials of high-temperature superconductors. *Phys. Rev. B* **2004**, *70*, 52501:1–52501:4.

8. Saadaoui, H.; Azzouz, M. Doping dependence of coupling between charge carriers and bosonic modes in the normal state of high- $T_C$  superconductors. *Phys. Rev. B* **2005**, *72*, 184518:1–184518:11.
9. Azzouz, M.; Hewitt, K.C.; Saadaoui, H. Dichotomy and pseudogap signature in the Raman response of high- $T_C$  cuprates. *Phys. Rev. B* **2010**, *81*, 174502:1–174502:4.
10. Azzouz, M. Calculation of the phase of hidden rotating antiferromagnetic order. *Physica C* **2012**, *480*, 34–36.
11. Mermin, N.D.; Wagner, H. Absence of ferromagnetism or antiferromagnetism in one- or two-dimensional isotropic heisenberg models. *Phys. Rev. Lett.* **1966**, *17*, 1133–1136.
12. Kyung, B. Mean-field study of the interplay between antiferromagnetism and d-wave superconductivity. *Phys. Rev. B* **2000**, *62*, 9083–9088.
13. Chakravarty, S.; Laughlin, R.B.; Morr, D.K.; Nayak, C. Hidden order in the cuprates *Phys. Rev. B* **2001**, *63*, 094503:1–094503:10.
14. Tsuei, C.C.; Kirtley, J.R. Pairing symmetry in cuprate superconductors. *Rev. Mod. Phys.* **2000**, *72*, 969–1016.
15. Bardeen, J.; Cooper, L.N.; Schrieffer, J.R. Theory of Superconductivity. *Phys. Rev.* **1957**, *108*, 1175–1204.
16. Tallon, J.L.; Loram, J.W. The doping dependence of  $T^*$ —What is the real high- $T_C$  phase diagram? *Physica C* **2001**, *349*, 53–68.
17. Chubukov, A.V.; Morr, D.K. Electronic structure of underdoped cuprates. *Phys. Rep.* **1997**, *288*, 355–387.
18. Yoshida, T.; Zhou, X.J.; Lu, D.H.; Komiya, S.; Ando, Y.; Eisaki, H.; Kakeshita, T.; Uchida, S.; Hussain, Z.; Shen, Z.-X.; *et al.* Low-energy electronic structure of the high- $T_C$  cuprates  $\text{La}_{2-x}\text{Sr}_x\text{CuO}_4$  studied by angle-resolved photoemission spectroscopy. *J. Phys. Condens. Matter* **2007**, *19*, 125209:1–125209:23.
19. Ronning, F.; Kim, C.; Feng, D.L.; Marshall, D.S.; Loeser, A.G.; Miller, L.L.; Eckstein, J.N.; Bozovic, I.; Shen, Z.-X. Photoemission evidence for a remnant fermi surface and a d-wavelike dispersion in insulating  $\text{Ca}_2\text{CuO}_2\text{Cl}_2$ . *Science* **1998**, *282*, 2067–2072.
20. Doiron-Leyraud, N.; Proust, C.; LeBoeuf, D.; Levallois, J.; Bonnemaïson, J.-B.; Liang, R.; Bonn, D.A.; Hardy, W.N.; Taillefer, L. Quantum oscillations and the Fermi surface in an underdoped high- $T_C$  superconductor. *Nature* **2007**, *447*, 565–568.
21. Sebastian, S.E.; Harrison, N.; Goddard, P.A.; Altarawneh, M.M.; Mielke, C.H.; Liang, R.; Bonn, D.A.; Hardy, W.N.; Andersen, O.K.; Lonzarich, G.G. Compensated electron and hole pockets in an underdoped high- $T_C$  superconductor *Phys. Rev. B* **2010**, *81*, 214524:1–214524:17.
22. Matsui, H.; Takahashi, T.; Sato, T.; Terashima, K.; Ding, H.; Uefuji, T.; Yamada, K. Evolution of the pseudogap across the magnet-superconductor phase boundary of  $\text{Nd}_{2-x}\text{Ce}_x\text{CuO}_4$ . *Phys. Rev. B* **2007**, *75*, 224514:1–224514:4.
23. Fauqué, B.; Sidis, Y.; Hinkov, V.; Pailhès, S.; Lin, C.T.; Chaud, X.; Bourges, P. Magnetic order in the pseudogap phase of high- $T_C$  superconductors. *Phys. Rev. Lett.* **2006**, *96*, 197001:1–197001:4.

24. Li, Y.; Balédent, V.; Barisic, N.; Cho, Y.; Fauqué, B.; Sidis, Y.; Yu, G.; Zhao, X.; Bourges, P.; Greven, M. Unusual magnetic order in the pseudogap region of the superconductor  $\text{HgBa}_2\text{CuO}_{4+\delta}$ . *Nature* **2008**, *455*, 372–375.
25. Chang, J.; Blackburn, E.; Holmes, A.T.; Christensen, N.B.; Larsen, J.; Mesot, J.; Liang, R.; Bonn, D.A.; Hardy, W.N.; Watenphul, A.; *et al.* Direct observation of competition between superconductivity and charge density wave order in  $\text{YBa}_2\text{Cu}_3\text{O}_{6.67}$ . *Nat. Phys.* **2012**, *8*, 871–876.
26. Shekhter, A.; Ramshaw, B.J.; Liang, R.; Hardy, W.N.; Bonn, D.A.; Balakirev, F.F.; McDonald, R.D.; Betts, J.B.; Riggs, S.C.; Migliori, A. Ultrasonic signatures at the superconducting and the pseudogap phase boundaries in YBCO cuprates. Available online: <http://arxiv.org/abs/1208.5810> (accessed on 7 May 2013).
27. Dean, M.P.M.; Springell, R.S.; Monney, C.; Zhou, K.J.; Bozovic, I.; Pereiro, J.; Dalla Piazza, B.; Ronnow, H.M.; Morenzoni, E.; van den Brink, J.; *et al.* Spin excitations in a single  $\text{La}_2\text{CuO}_4$  layer. *Nat. Mater.* **2012**, *11*, 850–854.

© 2013 by the author; licensee MDPI, Basel, Switzerland. This article is an open access article distributed under the terms and conditions of the Creative Commons Attribution license (<http://creativecommons.org/licenses/by/3.0/>).